J Solid State Electrochem (2008) 12:1589–1598
DOI 10.1007/s10008-008-0527-1

ORIGINAL PAPER

Selected electrochemical properties of Pd–Au alloys: hydrogen absorption and surface oxidation

M. Łukaszewski · A. Czerwiński

Received: 22 November 2007 / Revised: 10 January 2008 / Accepted: 1 February 2008 / Published online: 26 February 2008

Abstract Hydrogen absorption into and surface oxidation of Pd–Au alloys in acidic solutions were studied by cyclic voltammetry (CV) and chronoamperometry (CA) coupled with the electrochemical quartz crystal microbalance (EQCM). The influence of alloy bulk and surface composition on the process of oxidation of absorbed hydrogen was examined. The stresses induced by hydrogen insertion in Pd–Au alloys were compared with the case of pure Pd. The potential corresponding to the formation of a monolayer of surface oxide was determined for Pd–Au alloys of different surface states. Electrochemical dissolution of Pd–Au alloys was investigated.

Keywords Pd–Au alloys · Hydrogen absorption · Stresses · Surface oxide · Electrochemical dissolution · Electrochemical quartz crystal microbalance

Introduction

In the literature, there are numerous works on the electrochemistry of Pd–Au alloys [1–27]. Two main subjects were investigated, namely, the phenomenon of hydrogen absorption [1–6, 13] and the processes connected with surface oxidation [6–13, 15, 17, 19, 20]. The electrocatalytic properties of that system were also examined, e.g. oxidation of carbon monoxide [16, 17, 22], formaldehyde [3, 20, 21, 23, 24], formates [12, 20, 21, 23], methanol [22], PF_3 [18], oxygen reduction [26, 27] and hydrogen evolution [25]. However, despite such intensive studies, some aspects of the electrochemical behaviour of Pd–Au alloys have not been thoroughly explored.

Palladium and gold form a continuous series of face-centered cubic solid solutions with the lattice parameter varying almost linearly with alloy composition [28–31]. The Pd–Au system is homogeneous at normal conditions, but during anodic polarisation in acidic medium, the surface of Pd–Au electrodes becomes heterogeneous due to selective dissolution of Pd [6–13, 15, 17, 19, 20]. According to our recent results [6], Pd–Au electrodes containing more than approximately 30% Pd absorb hydrogen. For Pd-rich alloys the β phase (i.e. non-stoichiometric metal hydride) can be formed, whilst for lower Pd content, hydrogen is absorbed only as the α phase (i.e. solid solution of hydrogen in metal) [2, 32]. Various aspects of the electrochemical behaviour of Pd–Au alloys in acidic solutions have been described in detail in [6–9, 12–15].

In this work, we present some new results on the electrochemistry of Pd–Au alloys not reported in our earlier papers [6, 7]. We show the influence of alloy bulk and surface composition on hydrogen desorption from Pd–Au electrodes. We have determined the potential of surface oxide formation on Pd-rich phase in Pd–Au alloys. We have used the electrochemical quartz crystal microbalance to examine hydrogen absorption into and dissolution of Pd–Au alloys.

Experimental

All the experiments were performed at room temperature in 1 or 0.5 M H_2SO_4 solutions deoxygenated with an argon

M. Łukaszewski · A. Czerwiński (✉)
Department of Chemistry, Warsaw University,
Pasteura 1,
02-093 Warsaw, Poland
e-mail: aczerw@chem.uw.edu.pl

A. Czerwiński
Industrial Chemistry Research Institute,
Rydygiera 8,
01-793 Warsaw, Poland

stream. A platinum gauze and $Hg|Hg_2SO_4|H_2SO_4$ were used as the auxiliary and the reference electrodes, respectively. All potentials in the text and on the figures are referred to the RHE in the working solution. In the electrochemical quartz crystal microbalance (EQCM) experiments, 10 MHz AT-cut Au-plated crystals were used. The calibration constant determined by Ag and Pd deposition was 1.2 ng Hz^{-1}, very close to the theoretical value based on the Sauerbrey equation [33].

Pd–Au alloys were deposited potentiostatically on Au wires (0.5 mm diameter) from a bath containing $PdCl_2$ and $HAuCl_4$ in HCl [6, 7]. The concentrations of the salts in the bath were in the range 0.08–0.11 M $PdCl_2$ and 0.002–0.02 M $HAuCl_4$. The composition of the alloys was altered by employing different bath compositions and deposition potentials and utilising different dissolution rates of the metals during the procedure of potential cycling to high potentials [6–13, 15, 17, 19, 20]. The deposition potential was from the range 0.41–0.62 V, i.e. was always higher than the potential of hydrogen sorption to avoid hydrogen insertion into the alloy being formed. Lower deposition potential and higher concentration ratio between $PdCl_2$ and $HAuCl_4$ in the bath resulted in alloys containing more Pd in the bulk.

The thickness of alloy layers was in the range 2–3 μm for deposits on Au wires and approximately 0.3 μm for EQCM electrodes. The roughness factor of freshly deposited alloys was in the range 100–500 for deposits on Au wires and 40–70 for EQCM electrodes. Alloy real surface area was determined from surface oxide reduction charge and double layer capacity, according to procedures described earlier [7]. Bulk composition of Pd–Au alloys was obtained from the EDAX analysis (EDR-286 analyser coupled with LEO 435VP scanning electron microscope). In addition, the method based on the potential of α–β phase transition was also employed [34]. Surface composition of homogeneous samples was determined from the potential of surface oxides reduction peak, according to the method described by Rand and Woods [9]. In the case of superficially heterogeneous Pd–Au electrodes, the average composition was estimated from real areas occupied by each surface phase [7]. All alloy compositions are expressed in atomic percentages.

At the beginning of hydrogen electrosorption experiments, freshly prepared electrode was cycled continuously through the potential region of hydrogen adsorption and absorption until a steady-state voltammogram was obtained. This procedure was applied to avoid effects of ageing during further hydrogen insertion/removal. On the other hand, when surface oxidation processes were studied, potential cycling range was limited to the mere oxygen region.

Results and discussion

General cyclic voltammetric behaviour of Pd–Au EQCM electrodes

Figure 1 presents a cyclic voltammogram together with the EQCM response recorded for a Pd–Au alloy in 0.5 M H_2SO_4. Three main regions can be distinguished on the CV curve. In the so-called hydrogen region, hydrogen adsorption/absorption (a_1) and subsequent desorption (a_2) take place, whilst in the oxygen region, surface oxide formation (oxygen adsorption, c_1) and reduction (oxygen desorption, c_2) occur. These regions are separated by the double layer region (b), i.e. a potential range where no faradaic current flows. One should also note the multiple signals due to surface oxide reduction. According to Woods [8], it indicates surface heterogeneity of the sample, i.e. the existence of separate phases of different Pd surface content. Such behaviour is typical of Pd–Au alloys with moderate Pd content subjected after deposition to several potential cycles in the oxygen region [7]. The cathodic peak placed at the lowest potential (0.6 V) could be attributed to surface oxide reduction on a Pd-rich surface phase, the peak placed at intermediate potential (0.8 V) originates from surface oxide reduction on an alloy phase with higher Au content, whilst the peak at the highest potential (1.1 V) corresponds to surface oxide reduction on Au-rich phase. The analysis of the anodic part of the CV curve reveals two rather than three regions of current increase, which may be attributed to the onset of oxidation of surface atoms in the two phases with significant Pd concentration and atoms in the Au-rich phase, respectively. According to the literature [6–9, 12–15], the latter phase has electrochemical properties almost identical with those of pure gold and is oxidised at potential considerably higher than Pd-rich phases which probably start to be oxidised in a similar potential range and their signals overlap. Various types of CV curves for Pd–Au alloys of different compositions and after various ways of electrochemical treatment have been discussed in detail elsewhere [7].

The course of the frequency–potential curve can be explained on the basis of the earlier EQCM studies on noble metals and their alloys [35–38], taking into account that negative frequency shift corresponds to effective mass gain. In the anodic scan, the frequency initially increases with potential (1), which can be attributed to the oxidation of the absorbed hydrogen. Then frequency drops (2) due to the adsorption of anions followed by surface oxide formation on Pd-rich phase (above 0.75 V). At approximately 1.0 V, the frequency rises again (3), which probably reflects the electrochemical dissolution of Pd. Finally, another frequency decrease is observed (4), which is

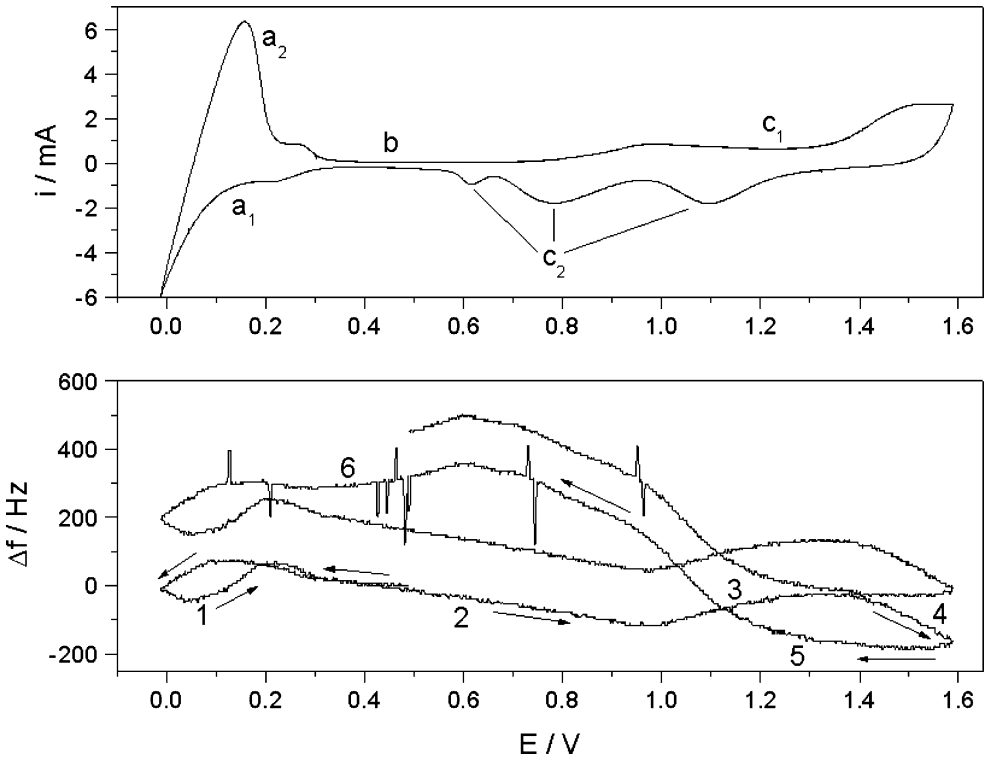

Fig. 1 Cyclic voltammogram and frequency–potential response for a heterogeneous Pd–Au alloy (38% Pd on the surface). Potential range −0.01÷1.59 V, scan rate 0.1 V s^{-1}, 0.5 M H_2SO_4

paralleled with surface oxide formation on Au-rich phase (see current increase above 1.35 V).

The fact of metal dissolution is confirmed by a frequency rise observed between two consecutive potential cycles indicating resultant mass loss. It should be added that the changes in the frequency–potential curve observed within even so small number of cycles were not accompanied by any noticeable changes in the course of the cyclic voltammogram. Our earlier studies demonstrated that during a single anodic scan, the amount of dissolved metal does not exceed a fraction of a monolayer of surface atoms [35]. However, with the use of such a sensitive device like the EQCM, it is possible to detect these subtle effects.

In the cathodic scan, frequency increases in the whole oxygen region as surface oxides are reduced (5). An interesting feature is frequency negative shift in the double layer region (6) where positive changes could be expected due to the desorption of anions as the electrode potential becomes less positive. However, the latter type of frequency course is observed only when the potential scan was started in the double layer region, i.e. without prior polarisation to the oxygen region. Therefore, it is possible that the observed mass gain in the cathodic scan is connected with a partial redeposition of metal dissolved previously in the anodic scan. To avoid the effects of metal dissolution/redeposition, during hydrogen absorption/desorption experiments the electrodes were not polarised to such high potentials.

It should be stressed that heterogeneity of the surface of Pd–Au alloys is not an equilibrium feature because these alloys form continuous series of solid solutions without a miscibility gap over the entire composition range and their surface compositions are normally close to the bulk compositions [19]. In fact, the surface segregation observed in our work is a result of the preferential dissolution of Pd during prolonged potential cycling in the oxygen region. Once the additional surface phases have appeared as a result of the electrochemical treatment, this surface state was maintained during further experiments, i.e. no re-homogenisation could be observed. In that sense, under the conditions of cyclic voltammetric experiments, heterogeneous Pd–Au alloys were more stable than homogeneous alloys. A detailed discussion on the changes of surface properties of Pd–Au alloys after electrochemical ageing has been presented in our earlier papers [6, 7].

Hydrogen absorption in Pd–Au alloys

Figure 2 shows the anodic voltammetric scans for oxidation of hydrogen absorbed at constant potential (corresponding to maximum saturation of the electrode with hydrogen) in Pd and Pd–Au alloys of various bulk Pd content. One should note that with the decrease in Pd bulk concentration, the potential of hydrogen oxidation peak is shifted negatively. It means that hydrogen removal from those alloys is facilitated in comparison with pure Pd. The reason

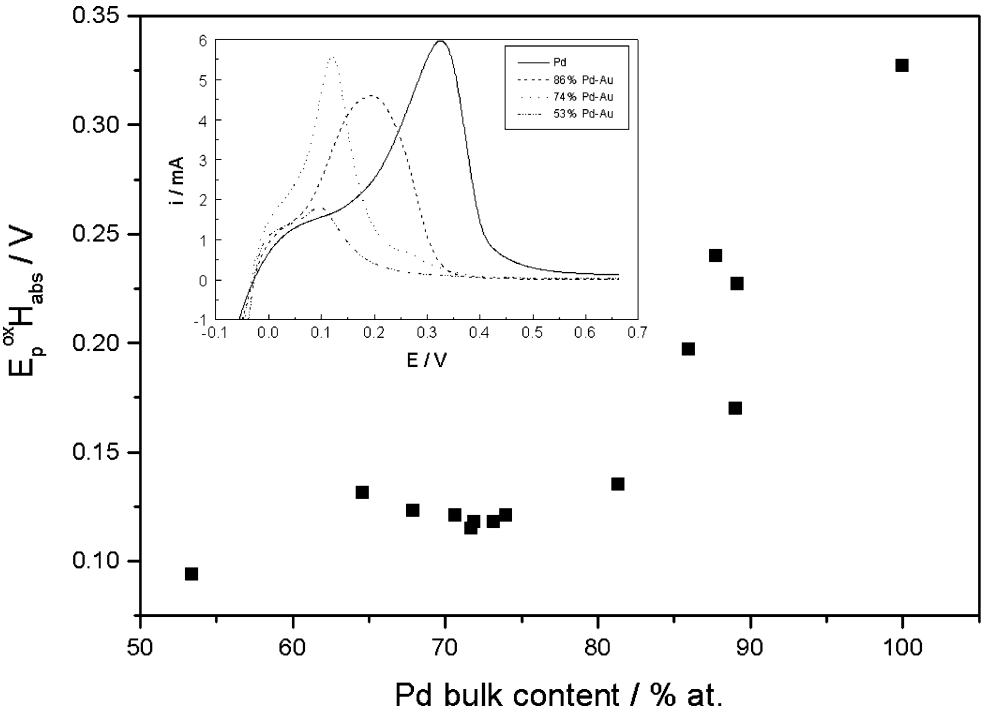

Fig. 2 Potential of absorbed hydrogen oxidation peak versus Pd bulk content in Pd–Au alloys. *Inset* absorbed hydrogen oxidation currents on Pd and Pd–Au alloys of various bulk compositions. Scan rate 0.01 V s^{-1}, 1 M H_2SO_4, hydrogen absorption at −0.13 V for 300 s, upper potential limit 0.67 V

may be the fact that Au addition to Pd changes both surface and bulk characteristics of the system, which influence its absorption properties. The process of hydrogen desorption is affected by such factors (dependent on alloy surface and bulk composition) as: surface coverage with adsorbed hydrogen, adsorbed hydrogen–metal bond energy, surface arrangement of atoms of particular alloy components, the rate of the α–β phase transition and hydrogen diffusion. It should be stressed that the effect observed for Pd–Au alloys is probably kinetic in origin because from the thermodynamic point of view, the β phase decomposition is shifted into higher potentials with the decrease in Pd bulk content due to crystal lattice expansion [2, 30, 32, 34]. Faster kinetics of hydrogen absorption in the alloy than in pure metal has already been reported for the Pd–Ag system [39].

Figure 3 presents a series of chronoamperograms recorded for a potential step from the double layer region (0.48 V) to different potentials from the hydrogen region. After negative potential jump, a current flows due to the reduction of H^+ ions to H atoms adsorbed on the surface, which subsequently enter the Pd crystal lattice forming a bulk phase of absorbed hydrogen (α or β phase, depending on potential applied). One should note that after a certain time, the reduction current reaches a steady value. For sufficiently low potentials, this value is determined by the rate of hydrogen evolution reaction taking place at the electrode surface, whilst for potentials too high for hydrogen evolution to occur, the current falls to zero, as can be expected for a thin Pd–Au layer fully saturated with hydrogen in a deoxygenated solution free from impurities.

From the chronoamperometric curves, it is possible to determine, for a given potential, the time needed to obtain steady-state electrode saturation with hydrogen (i.e. the time when current reaches a constant value). The *t–E* plot is presented in Fig. 3. It demonstrates that with a decrease in the electrode potential (and a simultaneous increase in the amount of absorbed hydrogen) the absorption time initially increases, passes through a sharp maximum and then decreases. The existence of the maximum on the *t–E* dependence indicates the potential where the rate of the absorption process reaches the minimum value. Similar behaviour was also observed for other Pd alloys: Pd–Pt [40], Pd–Rh [41], Pd–Pt–Rh [42], Pd–Ni [43] and pure Pd [42]. A comparison of the position of the time maximum with the dependence of the amount of absorbed hydrogen on potential reveals that this value lies within the phase transition region. Therefore, it can be suggested that the slow process of α–β transition rather than surface kinetics or bulk diffusion controls the overall rate of hydrogen absorption into thin Pd-based layers. Such possibility has already been postulated in the literature [44–46].

In our earlier studies on hydrogen absorption in Pd [47–49] and its alloys [6, 50], we have found that hydrogen desorption can proceed via two independent paths, namely, electrochemical oxidation and non-electrochemical recombination of adsorbed hydrogen. The latter effect is manifested in a cyclic voltammetric experiment as a decrease in the electrochemically measured amount of absorbed hydrogen at low scan rates (for discussion see [50]). One may suppose that the contribution of the non-

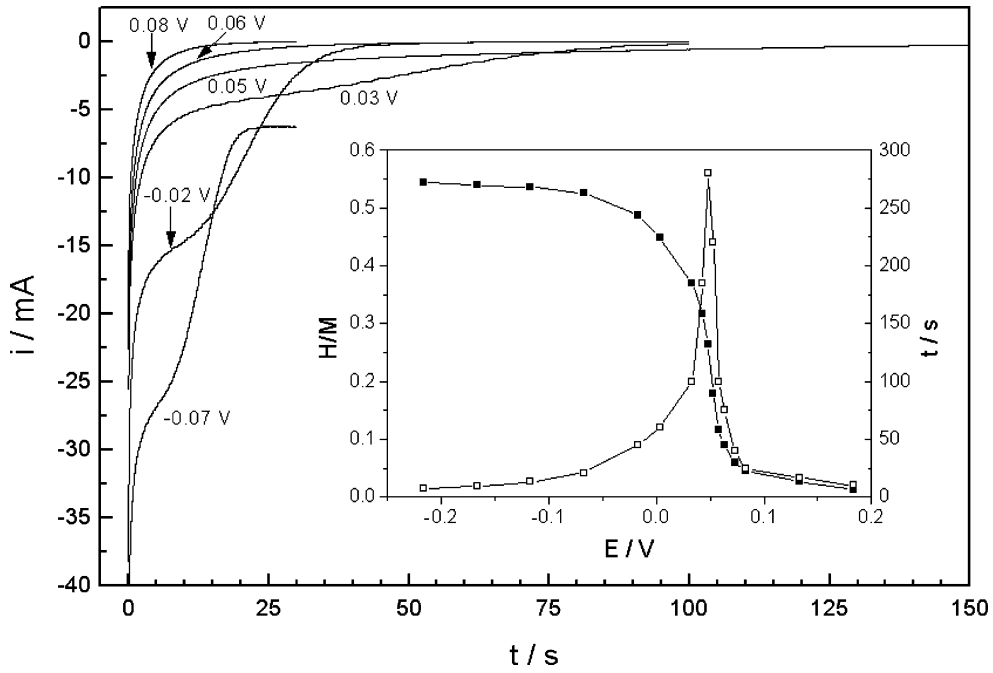

Fig. 3 Chronoamperograms recorded in 0.5 M H_2SO_4 during hydrogen electrosorption in a Pd–Au alloy (85% Pd in the bulk) at different potentials after pre-treatment at 0.48 V. *Inset* the amount of absorbed hydrogen (*solid symbols*), expressed as the hydrogen-to-metal ratio (H/M), and time needed for a steady-state electrode saturation with hydrogen (*open symbols*) versus absorption potential

electrochemical desorption path in the process of hydrogen removal from a Pd alloy should be strictly connected with surface composition and distribution of Pd atoms on the surface. In particular, it should depend on whether Pd atoms are randomly located or form islands. Because Au does not adsorb hydrogen, the process of non-electrochemical hydrogen desorption from a Pd–Au alloy should be effective only on conditions that there were sufficiently neighbouring Pd atoms on the electrode surface. Hydrogen adsorbed on isolated Pd sites, surrounded by Au atoms, might not be removed via recombination reaction. To verify this hypothesis, hydrogen desorption was performed on Pd–Au electrodes of similar bulk properties (approximately 80% Pd in the bulk) but of different surface states (reflected in the respective CV curves in Fig. 4) obtained by controlled potential cycling in the oxygen region: (1) Pd-rich homogeneous alloy (89% Pd on the surface), (2) heterogeneous alloy containing comparable amounts of Pd-rich and Au-rich phases (58% Pd on the surface) and (3) heterogeneous alloy strongly impoverished with Pd (10% Pd on the surface).

The obtained charge versus scan rate dependence confirms the above prediction that for a Pd-poor alloy the contribution of the non-electrochemical hydrogen desorption path is smaller than for a Pd-rich alloy. The lowering of hydrogen oxidation charge at low scan rates is the strongest for sample 1, for which a single surface oxide reduction peak observed on the CV curve mirrors alloy homogeneity and high Pd surface concentration. On the other hand, for sample 3, the significance of hydrogen recombination reaction is much lower, i.e. the decrease in hydrogen oxidation charge at low scan rates is less pronounced. In that case, the multiplicity of surface oxide reduction signal on CV curve reflects alloy surface heterogeneity. Moreover, the main cathodic peak originates from surface oxide reduction on Au-rich phase indicating low surface concentration of Pd. The influence of electrode surface state on the mechanism of hydrogen desorption was found earlier for the Pd–Pt–Rh system [50].

One could suppose that the above effects are caused by the influence of oxidation of molecular hydrogen (generated at absorption potential) on the total measured hydrogen charge. However, it should be stressed that as it was found in an earlier work performed in our laboratory [40], the oxidation of hydrogen generated during hydrogen evolution reaction has no significant influence on the total charge calculated from the oxidation peak used for the determination of the amount of absorbed hydrogen. Such assumption is justified by the fact that on voltammograms recorded in the hydrogen region for alloys not absorbing hydrogen, a pronounced hydrogen evolution current was observed as a cathodic signal but in the course of the anodic scan the oxidation current was negligible. Moreover, similar shape of charge versus scan rate dependence was also observed when hydrogen absorption was performed at potentials where hydrogen evolution does not occur (see discussion in [50]). Thus, it can be concluded that the main reason for the observed changes in hydrogen oxidation charge are different contributions from hydrogen recombination reaction on samples of different surface state.

Hydrogen absorption in Pd–Au alloys has also been studied using the EQCM. Figure 5 shows the relationship between frequency changes and the amount of hydrogen absorbed in Pd and a Pd–Au alloy. It is visible that for both samples the response of the quartz crystal resonator exceeds

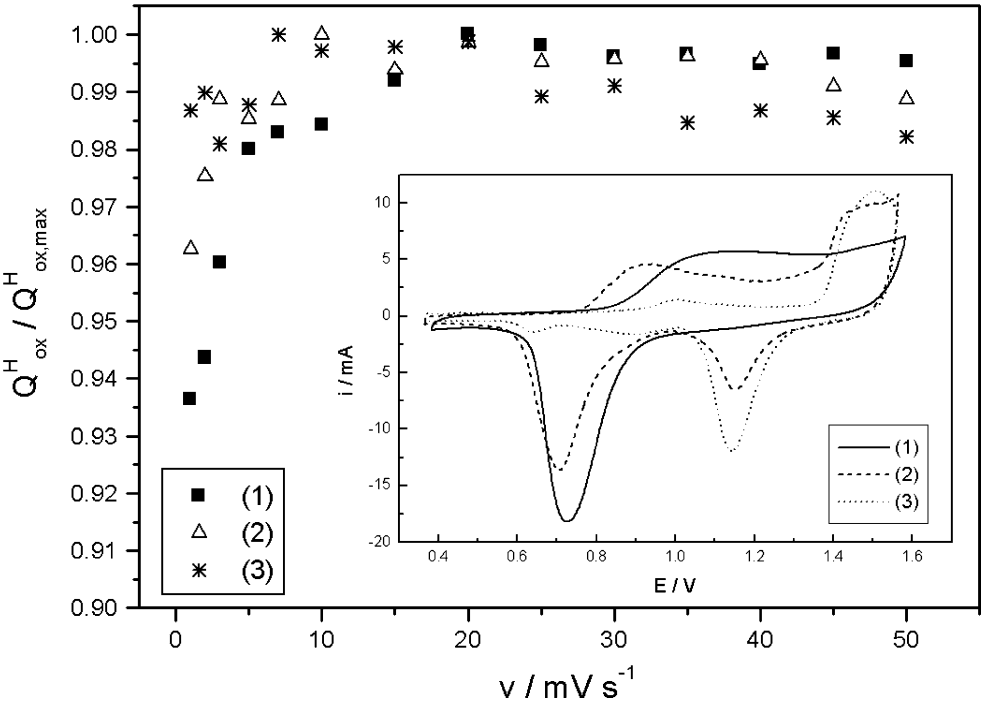

Fig. 4 Influence of scan rate on the charge (normalised to maximum value in a series) due to the oxidation of hydrogen absorbed at −0.03 V in Pd–Au alloys (approximately 80% Pd in the bulk) of various surface state: (*1*) homogeneous alloy (89% Pd on the surface), (*2*) heterogeneous alloy containing comparable amounts of Pd-rich and Au-rich phases (58% Pd on the surface) and (*3*) heterogeneous alloy strongly impoverished with Pd (10% Pd on the surface). *Inset* cyclic voltammograms (0.1 V s^{-1}, 1 M H_2SO_4) in the oxygen region (0.37÷1.57 V) for the alloys examined

the value expected for pure mass effect predicted on the basis of the Sauerbrey equation (dashed line in Fig. 5). It corresponds to the known fact that frequency changes observed in hydrogen absorption experiments originate not only from mass gain due to hydrogen uptake but also from stresses in crystal lattice induced by that process [36, 37, 39, 51–63]. Thus, although the amount of absorbed hydrogen cannot be determined directly from frequency measurements [60, 61], the EQCM can be utilised for the studies of stress effects accompanying hydrogen insertion.

As can be seen in Fig. 5, frequency decreases with the increase in the amount of absorbed hydrogen and the rate of frequency changes is slower for a Pd–Au alloy than for Pd. It means that the stress effect, reflected in the deviation from the Sauerbrey equation, is smaller for the alloy than for pure metal. These differences are confirmed by the values of apparent molar mass of hydrogen absorbed in the β phase, which are 1.9 g mol^{-1} for the alloy and 3 g mol^{-1} for Pd. The latter value is in agreement with most authors [51, 55, 56, 60, 61], although other authors reported

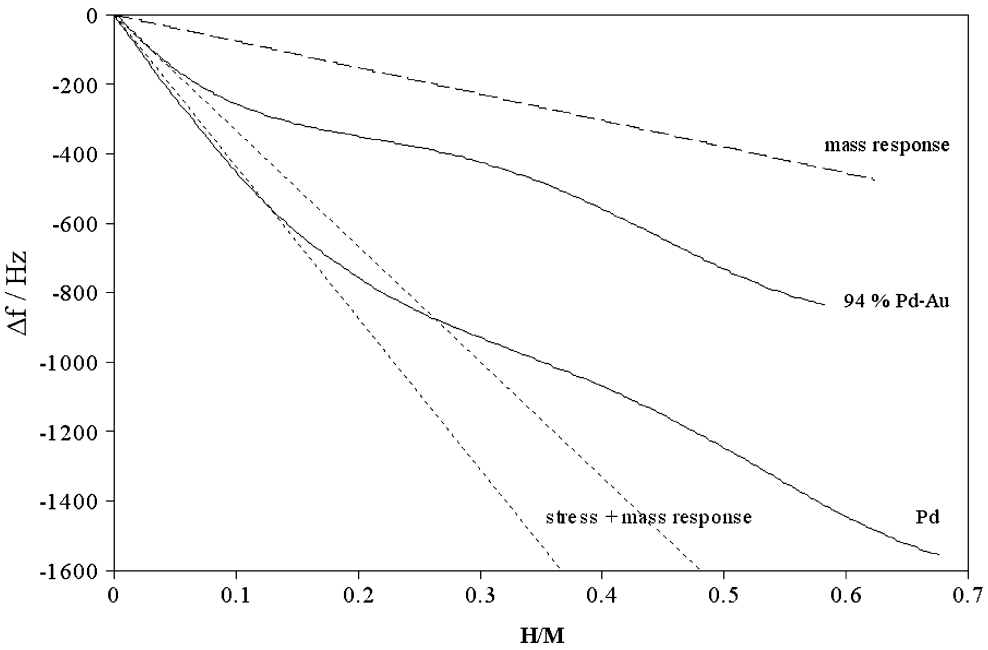

Fig. 5 *Solid lines* frequency changes versus the amount of hydrogen absorbed in Pd and a Pd–Au alloy (94% Pd in the bulk) obtained in chronoamperometric experiment (potential step from 0.39 to 0.01 V) in 0.5 M H_2SO_4. *Dashed line* resonator response predicted for pure mass effect. *Dotted lines* responses predicted for mass and stress effects together

different values [59]. However, the differences between or agreements with various literature data might be explained by different values of the lattice stresses for various structures of palladium prepared using different methods. Because our Pd and Pd–Au electrodes were obtained according to similar procedures, the values of apparent molar mass can be compared. Again, the deviation of apparent molar mass from the real molar mass of hydrogen, i.e. 1 g mol^{-1}, is a measure of the stress effects [36, 37, 59–61, 63]. Such behaviour is qualitatively consistent with crystallographic data [2, 32], according to which the relative increase in lattice parameter during β phase formation becomes smaller upon Pd alloying with Au. Also for other expanded system, i.e. Pd–Ag, the stresses were smaller than in pure Pd [39].

To analyse the EQCM response more quantitatively, the total frequency shift was calculated as a sum of mass effect (via the Sauerbrey equation from charge consumed during hydrogen uptake) and the stress effect. In the latter case, an average stress was obtained as a product of Young's modulus [64] and lattice parameter expansion during the β phase formation [2, 32]) and then recalculated into stress-related frequency shift (Δf_{stress}) according to the equation [39, 58]:

$$\Delta f_{\mathrm{stress}} = \left(\tau \times k \times f_{\mathrm{q}} \times t_{\mathrm{f}}\right)/t_{\mathrm{q}} \quad (1)$$

where τ is the average stress in a thin film of thickness t_f (in this study, 0.3 μm), k is the stress coefficient (-2.75×10^{-11} m^2 N^{-1} for AT-cut crystals), f_q is the fundamental frequency of the quartz crystal (in this study, 10 MHz) and t_q is the thickness of the quartz crystal (166 μm for 10 MHz). The results show that only for low hydrogen content the measured resonator response coincide with the predicted values (dotted lines in Fig. 5), whilst for higher amounts of hydrogen positive deviations are observed. The possible reason for such discrepancies may be changes in elastic properties of the metal/alloy after absorption of a certain amount of hydrogen. Similar effect was reported for thin Nb films electrolytically loaded with hydrogen [65, 66]. The change in slope of the stress versus concentration curve was attributed to the onset of plastic deformation [65] leading to stress release by means of dislocation generation that sets in above a certain hydrogen concentration [66].

Anodic oxidation of Pd–Au alloys

At potentials considerably higher than those corresponding to hydrogen-related phenomena, the surface of noble metal electrodes undergoes oxidation, which involves surface oxide formation and electrochemical dissolution of the electrode material. In our earlier papers [6, 7], we have discussed changes in the surface state of Pd–Au alloys caused by repetitive potential cycling through the oxygen region. We have stated that on Pd–Au electrodes strongly impoverished with Pd the main surface phase has electrochemical properties very similar to those typical of pure Au. Below, we present the results on anodic oxidation of Pd-rich Pd–Au alloys.

Figure 6a–e shows the dependence of surface oxide reduction charge on the upper potential limit in cyclic voltammetric experiment (scan rate 0.1 V s^{-1}) for Pd and Pd–Au alloys of different surface states. In the case of heterogeneous alloys (i.e. exhibiting separate peaks originating from surface oxide reduction on particular surface phases), the peak corresponding to surface oxide formation on Pd-rich phase (i.e. alloy phase) was considered. As can be seen in Fig. 6a–e, the amount of surface oxide increases almost linearly with the upper potential limit, and for a certain potential value, a change in the Q–E slope is observed. According to the literature [8, 67–69], this inflexion point can be attributed to the formation of a monolayer of surface oxide. One should note that the value of the potential of surface oxide monolayer formation on Pd–Au electrodes is higher than on pure Pd and increases with the decrease in Pd concentration in the alloy phase (Fig. 6f), i.e. as the electrode surface becomes more noble. Thus, it confirms earlier statements [7–10] that metal adsorption properties towards oxygen are significantly modified upon Pd alloying with Au. The intermediate potential of surface oxide monolayer formation suggests that atomic interactions in the alloy are sufficient to make average the adsorption characteristics of these two metals [7–10]. It means that a real alloy phase is formed whose electrochemical behaviour is different from that of pure components.

Another reaction that proceeds at sufficiently anodic potentials, especially in acidic solutions, is electrochemical dissolution of the electrode material. We have studied this phenomenon by the EQCM method. Pd–Au electrode was polarised in the oxygen region to various upper potential limits and the mass of dissolved metal was calculated (via the Sauerbrey equation) from the difference in frequency between two consecutive anodic scans measured at the upper potential limit (see Fig. 1). Figure 7 presents the dependence of the amount of dissolved metal (per unit of alloy real surface area) on the upper potential limit. One can see a monotonic increase in the mass lost with increasing electrode potential. The influence of scan rate on the dissolution effect is also visible.

According to the literature [70], under conditions applied in our experiments, mainly Pd dissolution is expected because Au is much more resistive to that process. To verify this hypothesis, the amount of metal dissolved from the Pd–Au alloy was recalculated per Pd area only and compared with the data for pure Pd (see inset in Fig. 7). It is clearly demonstrated that both series of data coincide, confirming the above assumption. In Fig. 8, the frequency

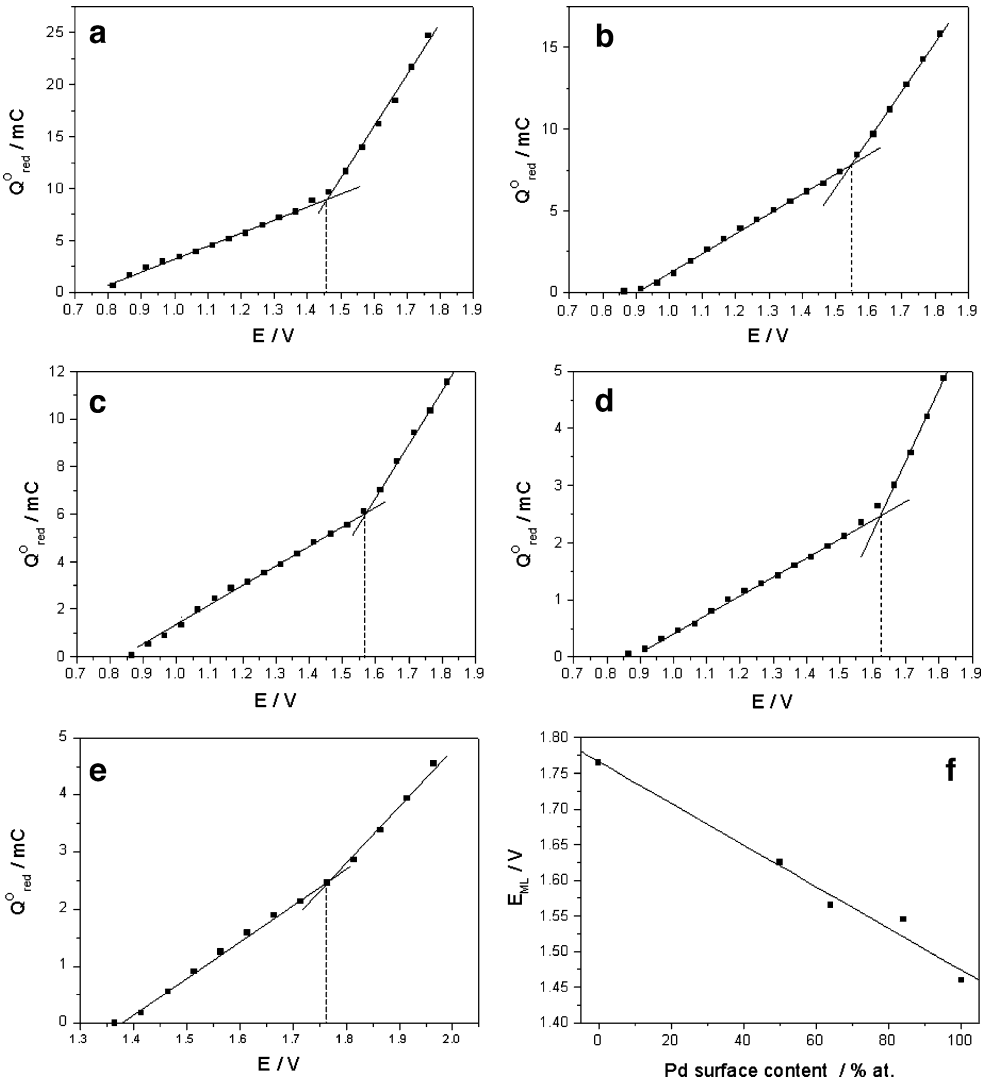

Fig. 6 Charge of surface oxide reduction peak versus upper potential limit for electrodes of various constitutions: **a** pure Pd, **b** homogeneous Pd–Au alloy containing 84% Pd on the surface, **c** heterogeneous Pd–Au alloy with a Pd-rich surface phase containing 64% Pd, **d** heterogeneous Pd–Au alloy with a Pd-rich surface phase containing 50% Pd, **e** pure Au. *Vertical lines* indicate the potential of surface oxide monolayer formation. **f** Potential of surface oxide monolayer formation versus Pd surface content. Scan rate 0.1 V s^{-1}, 1 M H_2SO_4

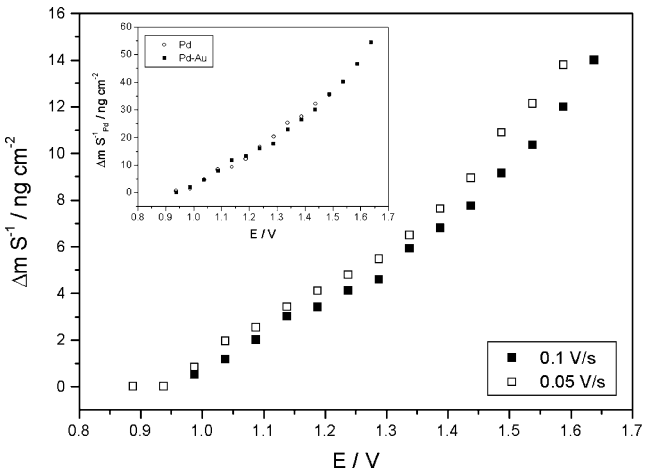

Fig. 7 Mass of dissolved metal per the unit of alloy real surface area versus upper potential limit for a Pd–Au alloy (26% Pd on the surface) polarised in 0.5 M H_2SO_4 with two scan rates (0.1 and 0.05 V s^{-1}). *Inset* mass of dissolved metal recalculated per Pd surface area versus upper potential limit for pure Pd and a Pd–Au alloy (0.1 V s^{-1})

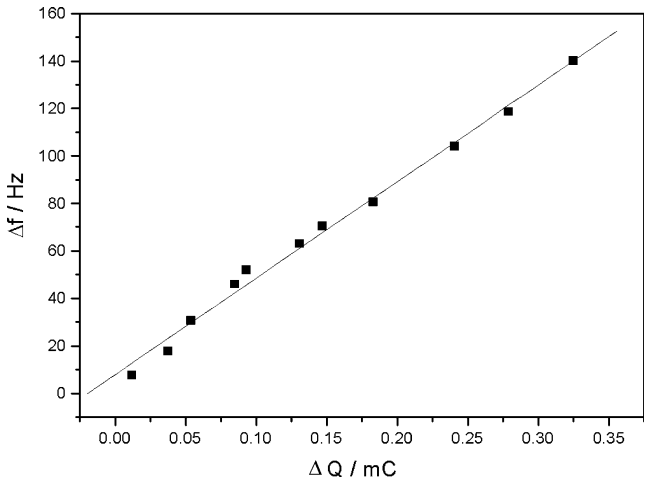

Fig. 8 Frequency shift between two consecutive voltammetric cycles versus difference between total anodic and cathodic charges for a Pd–Au alloy (26% Pd on the surface). Scan rate 0.1 V s^{-1}, 0.5 M H_2SO_4

shift between two consecutive cycles was correlated with the difference in total charges in anodic and cathodic voltammetric scans. A straight line was obtained with a slope giving Pd valency of 2.2, i.e. indicating its oxidation to Pd^{2+} ions.

Conclusions

The potential of absorbed hydrogen oxidation peak is shifted negatively with a decrease in Pd bulk content. The effect of non-electrochemical desorption of absorbed hydrogen depends on alloy surface state and becomes weaker after alloy impoverishment with Pd. The stresses induced by hydrogen insertion in Pd–Au alloys are smaller than in pure Pd. The potential corresponding to the formation of a monolayer of surface oxide on Pd–Au alloys is shifted positively with a decrease in Pd surface content. EQCM results confirm that mainly Pd is dissolved from Pd–Au alloys subjected to polarisation to the potentials of the oxygen region.

Acknowledgment This research was financed within a framework of 6FP HydroNanoPol project and a SPB HydroNanoPol project financially supported by the Ministry of Science and Higher Education (MNiSW).

References

1. Gray TJ, Rozelle RB, Soeder ML (1964) Nature 202:181
2. Maeland A, Flanagan TB (1965) J Phys Chem 69:3575
3. Machida K, Enyo M (1987) J Electrochem Soc 134:1472
4. Hoare JP, Castellan GW, Schuldiner S (1958) J Phys Chem 62:1141
5. Pyun S-I, Lee W-J, Yang T-H (1997) Thin Solid Films 311:183
6. Łukaszewski M, Kuśmierczyk K, Kotowski J, Siwek H, Czerwiński A (2003) J Solid State Electrochem 7:69
7. Łukaszewski M, Czerwiński A (2003) Electrochim Acta 48:2435
8. Woods R (1976) Chemisorption at electrodes. In: Bard AJ (ed) Electroanalytical chemistry. vol. 9. Marcel Dekker, New York, pp 2–162
9. Rand DAJ, Woods R (1972) J Electroanal Chem 36:57
10. Rand DAJ, Woods R (1974) Surf Sci 41:611
11. Conway BE, Angerstein-Kozlowska H, Czartoryska G (1978) Z Phys Chem 112:195
12. Beden B, Lamy C, Leger J-M (1979) Electrochim Acta 24:1157
13. Woods R (1969) Electrochim Acta 14:632
14. Gossner K, Mizera E (1981) J Electroanal Chem 125:359
15. Gossner K, Mizera E (1982) J Electroanal Chem 140:47
16. Gossner K, Mizera E (1979) J Electroanal Chem 98:37
17. Gossner K, Mizera E (1982) J Electroanal Chem 140:35
18. Gossner K, Mizera E (1986) J Electroanal Chem 201:397
19. Nishimura K, Machida K, Enyo M (1988) J. Electroanal Chem 257:217
20. Nishimura K, Machida K, Enyo M (1988) J Electroanal Chem 251:103
21. Nishimura K, Machida K, Enyo M (1988) J Electroanal Chem 251:117
22. Nishimura K, Machida K, Enyo M (1989) J Electroanal Chem 260:167
23. Nishimura K, Kunimatsu K, Machida K, Enyo M (1989) J Electroanal Chem 260:181
24. Enyo M (1985) J Electroanal Chem 186:155
25. Schuldiner S, Hoare JP (1957) J Phys Chem 61:705
26. Damjanovic A, Brusić V (1967) J Electroanal Chem 15:29
27. Damjanovic A, Brusić V (1967) Electrochmi Acta 12:1171
28. Pearson WB (1958) A handbook of lattice spacings and structures of alloys. Pergamon, London
29. Hansen M (1958) Constitution of binary alloys. McGraw-Hill, New York
30. Lewis FA (1967) The palladium–hydrogen system. Academic, London
31. Su F-Y, Huang J-F, Sun I-W (2004) J Electrochem Soc 151:C811
32. Sakamoto Y, Yuwasa K, Hirayama K (1982) J Less-Common Met 88:115
33. Sauerbrey G (1959) Z Phys 155:206
34. Łukaszewski M, Żurowski A, Grdeń M, Czerwiński A (2007) Electrochem Commun 9:671
35. Łukaszewski M, Czerwiński A (2006) J Electroanal Chem 589:38
36. Łukaszewski M, Czerwiński A (2006) J Electroanal Chem 589:87
37. Łukaszewski M, Czerwiński A (2007) Pol J Chem 81:847
38. Łukaszewski M, Siwek H, Czerwiński A (2007) Electrochim Acta 52:4560
39. Liu S-Y, Kao Y-H, Oliver Su Y, Perng T-P (1999) J Alloys Compd 293–295:468
40. Grdeń M, Piaścik A, Koczorowski Z, Czerwiński A (2002) J Electroanal Chem 532:35
41. Żurowski A, Łukaszewski M, Czerwiński A (2006) Electrochim Acta 51:3112
42. Łukaszewski M, Grdeń M, Czerwiński A (2004) J Electroanal Chem 573:87
43. Grdeń M, Kuśmierczyk K, Czerwiński A (2002) J Solid State Electrochem 7:43
44. Zhang W-S, Zhang X-W, Zhao X-G (1998) J Electroanal Chem 458:107
45. Millet P, Srour M, Faure R, Durand R (2001) Electrochem Commun 3:478
46. Bennett PA, Fuggle JC (1982) Phys Rev B 26(11):6030
47. Czerwiński A, Kiersztyn I, Grdeń M, Czapla J (1999) J Electroanal Chem 471:190
48. Czerwiński A, Kiersztyn I, Grdeń M (2000) J Electroanal Chem 492:128
49. Czerwiński A, Kiersztyn I, Grdeń M (2003) J Solid State Electrochem 7:321
50. Czerwiński A, Grdeń M, Łukaszewski M (2004) J Solid State Electrochem 8:411
51. Bucur RV, Flanagan TB (1974) Z Phys Chem 88:225
52. Bucur RV, Mecea V, Flanagan TB (1976) Surf Sci 54:477
53. Lee M-W, Glosser R (1985) J Appl Phys 57:5236
54. Gräsjo L, Seo M (1990) J Electroanal Chem 296:233
55. Cheek GT, O'Grady WE (1990) J Electroanal Chem 277:341
56. Cheek GT, O'Grady WE (1994) J Electroanal Chem 368:133
57. Liu S-Y, Kao Y-H, Oliver Su Y, Perng T-P (2000) J Alloys Compd 311:283
58. Liu S-Y, Kao Y-H, Oliver Su Y, Perng T-P (2001) J Alloys Compd 316:280
59. Gabrielli C, Grand PP, Lasia A, Perrot H (2002) Electrochim Acta 47:2199
60. Grdeń M, Kotowski J, Czerwiński A (1999) J Solid State Electrochem 3:348
61. Grdeń M, Kotowski J, Czerwiński A (2000) J Solid State Electrochem 4:273
62. Yamamoto N, Ohsaka T, Terashima T, Oyama N (1990) J Electroanal Chem 296:463

63. Grdeń M, Klimek K, Czerwiński A (2006) Electrochim Acta 51:2221
64. Fabre A, Finot E, Demoment J, Contreras S (2003) J Alloys Compd 356–357:372
65. Laudahn U, Pundt A, Becker M, v Hülsen U, Geyer U, Wagner T, Kirchheim (1999) J Alloys Compd 293–295:490
66. Pundt A (2004) Adv Eng Mater 6:11
67. Kuśmierczyk K, Łukaszewski M, Rogulski Z, Siwek H, Kotowski J, Czerwiński A (2002) Pol J Chem 76:607
68. Bolzán AE (1995) J Electroanal Chem 380:127
69. Brummer SB, Makrides AC (1964) J Electrochem Soc 111:1122
70. Rand DAJ, Woods R (1972) J Electroanal Chem 35:209